A Variable-Decoupling- and MSR-Based Imaging Algorithm for a SAR of Curvilinear Orbit

ARTICLE *in* IEEE GEOSCIENCE AND REMOTE SENSING LETTERS · NOVEMBER 2011

Impact Factor: 2.1 · DOI: 10.1109/LGRS.2011.2158387 · Source: DBLP

Mengdao Xing

Xidian University

Yong Wang

Nanjing University of Posts and Telecomm…

A Variable-Decoupling- and MSR-Based Imaging Algorithm for a SAR of Curvilinear Orbit

Peng Zhou, Mengdao Xing, Tao Xiong, Yong Wang, and Lei Zhang

***Abstract*—For a synthetic aperture radar (SAR) onboard a platform with a rectilinear track, the range history of a point target can be accurately expressed hyperbolically. The track can be curvilinear for a maneuverable SAR platform. The hyperbolic equation becomes inadequate, and an expression with high-order terms is needed. Using the method of series reversion, we derived the 2-D spectrum for the return signal of the curvilinear SAR. There were five independent variables in the spectrum, but available imaging algorithms could only handle three in the focusing using the spectrum. Thus, a variable-decoupling method was developed to reparameterize the initial spectrum so that only three variables remained. After the incorporation of the decoupling method into the chirp-scaling algorithm, simulations of the SAR with a curvilinear track were studied. Promising results were obtained.**

***Index Terms*—Chirp-scaling (CS) algorithm, method of series reversion (MSR), synthetic aperture radar (SAR) of rectilinear or curvilinear track, 2-D spectrum.**

I. Introduction

A SYNTHETIC aperture radar (SAR) mounted on a maneuverable platform exhibits a curvilinear flight path. The range history of a point target cannot be expressed accurately using a hyperbolical function. An expression with higher order terms is needed. Thus, not only the history becomes complicated but also the validity of imaging algorithms based on the hyperbolical function could become questionable. To study the complicated range history, one corrects the curved flight path to a straight line [1] and then uses the hyperbolical function in the derivation of the 2-D spectrum or derives the 2-D spectrum using the complex range history [2]. The second type of approaches is popular now because of the direct use of the range history and efficiency. Thus, we focus on the second type of approaches.

Once the range history from the curvilinear flight path is expressed as a function with higher order terms, the method of series reversion (MSR) [3] can be useful in the derivation of the 2-D spectrum [4]. There are five independent variables coupled in the MSR-derived 2-D spectrum. They are the range frequency, azimuth frequency, slant range, and x and y coordinates of a ground target. Unfortunately, current and available imaging algorithms can only handle the first three. None can be directly applied to the spectrum that is of two extra coupled variables. In the derivation of the 2-D spectrum, Yi *et al.* [4] replaced the x and y coordinates with the coordinates of a beam center. This approach works fine when the radar is narrow in beamwidth but deteriorates greatly when a wide imaging region is needed. Therefore, a variable-decoupling method was investigated. The main idea of the decoupling includes the establishment of a one-to-one relationship between the instantaneous range of a ground target at zero azimuth time and each extra variable using the concept of instantaneous Doppler frequency (IDF). After the decoupling, a new 2-D spectrum with only three variables is acquired. Thus, available imaging algorithms can be used to process the data. Simulation results show that our method focuses and performs well when the imaging region is wide in range. Details are given next.

Manuscript received February 27, 2011; revised April 14, 2011; accepted May 24, 2011. Date of publication July 12, 2011; date of current version October 28, 2011. This work was supported by the Chinese “973” Program under Grant 2010CB731903 to Xidian University, Xi’an, China, as well as by the AmericaView to the East Carolina University under grant #211654.

P. Zhou, M. Xing, T. Xiong, and L. Zhang are with the National Key Laboratory of Radar Signal Processing, Xidian University, Xi’an 710071, China (e-mail: zhoupeng_993@hotmail.com).

Y. Wang is with the Department of Geography, East Carolina University, Greenville, NC 27858-4353 USA (e-mail: WANGY@ecu.edu).

Digital Object Identifier 10.1109/LGRS.2011.2158387

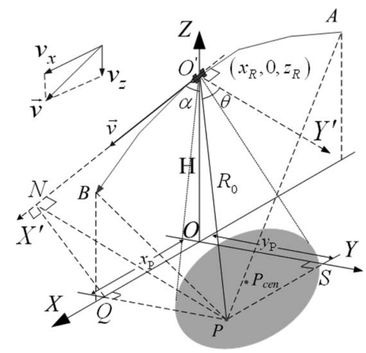

Fig. 1. Geometry of a maneuverable SAR platform.

II. Geometry of a Maneuverable SAR Platform, and an MSR-Based 2-D Spectrum

The geometry of a maneuverable SAR platform is shown in Fig. 1. The SAR is traveling along $\widehat{AB}$ in plane XOZ. Let t_m be azimuth time. Assume that, at $t_m = 0$, the sensor is at position O' with a height of H. The projection of O' on XOY or ground is origin O. $\vec{v} = (v_{x0}, 0, v_{z0})$ and $\vec{a} = (\alpha_x, 0, \alpha_z)$ denote the velocity and acceleration vectors of the sensor at that time, respectively. Therefore, the location of the sensor at t_m is $(v_{x0}t_m + 0.5\alpha_x t_m^2, 0, H + v_{z0}t_m + 0.5\alpha_z t_m^2)$. Let P be a ground target with coordinates $(x_P, y_P, 0)$. P_{cen} is a reference target located at the beam center. R_0 is the instantaneous distance between the sensor and P at $t_m = 0$, and $R(t_m)$ is the range history of P. Thus, backscattering from P can be written as

$$s(\hat{t}, t_m) = w_r\left(\hat{t} - \frac{2R(t_m)}{c}\right) w_a(t_m) \exp\left[-j\frac{4\pi}{\lambda}R(t_m)\right] \bullet \exp\left[j\pi\gamma\left(\hat{t} - \frac{2R(t_m)}{c}\right)^2\right] \quad (1)$$

where $\hat{t}$ is the range time, λ is the wavelength, c is the speed of light, and γ is the chirp rate. $w_r(\bullet)$ and $w_a(\bullet)$ are the range and azimuth envelopes, respectively.

To obtain the 2-D spectrum of $s(\hat{t}, t_m)$ analytically, we use a 2-D Fourier transform. During the derivation, the principle of stationary phase is adapted. The degree of complexity in the derivation largely depends on the expression of $R(t_m)$. For the SAR of rectilinear orbit

$$R(t_m) = \sqrt{R_0^2 + (x_P - |\vec{v}|t_m)^2} \quad (2)$$

applying (2) into (1), one can obtain its 2-D spectrum ([5, Ch. 5]). However, for the SAR of curvilinear orbit, we have (3), shown at the bottom of the page, with

$$\left.\begin{array}{ll} R_0 = \sqrt{x_p^2 + y_p^2 + H^2} & \\ \mu_1 = -2(v_{x0}x_p - v_{z0}H) & \mu_2 = v_{x0}^2 + v_{z0}^2 - a_x x_p + a_z H \\ \mu_3 = v_{x0}a_x + v_{z0}a_z & \mu_4 = \frac{1}{4}\left(a_x^2 + a_z^2\right) \end{array}\right\}. \quad (4)$$

Equation (3) is more complex than (2). This complexity causes a sixth-degree polynomial equation with respect to t_m that needs to be solved in the derivation of the Fourier integral [6], and one cannot solve the equation algebraically. Alternatively, the MSR [3] is introduced to derive the 2-D spectrum of $s(\hat{t}, t_m)$.

Using the Taylor expansion, one can express (3) as

$$R(t_m) \approx R_0 + b_1 t_m + b_2 t_m^2 + b_3 t_m^3 + b_4 t_m^4 \quad (5)$$

with

$$\left.\begin{array}{ll} b_1 = \frac{\mu_1}{2R_0} & b_2 = \frac{\mu_2}{2R_0} - \frac{\mu_1^2}{8R_0^3} \\ b_3 = \frac{\mu_3}{2R_0} - \frac{\mu_1\mu_2}{4R_0^3} + \frac{\mu_1^3}{16R_0^5} & b_4 = \frac{\mu_4}{2R_0} - \frac{2\mu_1\mu_3 + \mu_2^2}{8R_0^3} \\ & \quad + \frac{3\mu_1^2\mu_2}{16R_0^5} - \frac{5\mu_1^4}{128R_0^7} \end{array}\right\}. \quad (6)$$

Then, the MSR-based 2-D spectrum [4] is

$$S_{\text{MSR}} = w_r(f_r)w_a(f_a)\exp\left[-j\pi\frac{f_r^2}{\gamma}\right]\exp[j\Phi] \quad (7)$$

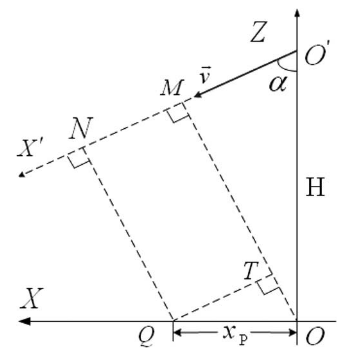

Fig. 2. Geometry in plane $O'OX$.

where f_r is the range frequency and f_a is the azimuth frequency. The second phase term

$$\begin{aligned} \Phi = & -4\pi\frac{R_0}{c}(f_r + f_c) \\ & + \pi\frac{c}{4b_2}\frac{1}{(f_r + f_c)}\left(f_a + (f_r + f_c)\frac{2b_1}{c}\right)^2 \\ & + \pi\frac{c^2 b_3}{16b_2^3}\frac{1}{(f_r + f_c)^2}\left(f_a + (f_r + f_c)\frac{2b_1}{c}\right)^3 \\ & + \pi\frac{c^3\left(9b_3^2 - 4b_2b_4\right)}{256b_2^5}\frac{1}{(f_r + f_c)^3}\left(f_a + (f_r + f_c)\frac{2b_1}{c}\right)^4. \end{aligned} \quad (8)$$

From (4) and (7), one finds that the MSR-based 2-D spectrum S_{MSR} is a function of five independent variables, namely, f_r, f_a, R_0, x_P, and y_P. Thus, S_{MSR} can be generally expressed as

$$S_{\text{MSR}} = S_{\text{MSR}}(f_r, f_a, R_0, x_P, y_P). \quad (9)$$

It should be noted that, for a SAR with a rectilinear orbit, the 2-D spectrum only consists of variables f_r, f_a, and R_0, and a typical imaging algorithm (e.g., the chirp-scaling (CS) algorithm) can be applied to process the spectrum. However, there are two extra variables x_P and y_P for a SAR of curvilinear track. As a result, none of the available imaging algorithms can be applied to process S_{MSR} directly. Thus, a variable-decoupling method is pursued next.

III. Decoupling Method

A. Decoupling y_P

y_P is only in the expression of R_0, the first equation in (4). Thus, if one just treats R_0 as an independent variable (but not a function of y_P) and considers y_P as an inherent component of R_0, y_P is decoupled in (9). Also, R_0, as a whole, can be calculated using radar parameters so that the decoupling of y_P from the 2-D spectrum is feasible.

$$\begin{aligned} R(t_m) &= \sqrt{\left(v_{x0}t_m + 0.5a_x t_m^2 - x_p\right)^2 + y_p^2 + \left(H + v_{z0}t_m + 0.5a_z t_m^2\right)^2} \\ &= \sqrt{R_0^2 + \mu_1 t_m + \mu_2 t_m^2 + \mu_3 t_m^3 + \mu_4 t_m^4} \end{aligned} \quad (3)$$

B. Decoupling x_P

To decouple x_P, one needs to use the concept of IDF of target P to create a new relationship between x_P and R_0. In Fig. 1, $O'N$ is the extended line along the moving direction of $\vec{v}$ at $t_m = 0$. Draw line QN, and let $QN \perp O'N$. Because $PQ \perp XOZ$, then $PQ \perp O'N$. Thus, $O'N \perp \Delta PQN$, and $O'N \perp PN$. After the establishment of new coordinates $X'O'Y'$ on the plane where $\Delta O'PN$ exists, one obtains the squint angle θ. Therefore, the expression of the IDF of P is

$$f_{\mathrm{id}} = \frac{2|\vec{v}|}{\lambda}\sin\theta = \frac{2|\vec{v}|}{\lambda}\sin\left(\frac{\pi}{2} - \angle PO'N\right) = \frac{2|\vec{v}|}{\lambda}\sin\left(\frac{\pi}{2} - \arccos\left(\frac{O'N}{R_0}\right)\right) \tag{10}$$

where $O'N$ is unknown, whereas the rest of the parameters are known. To solve $O'N$, we redraw plane $O'OX$ as in Fig. 2. Add line OM perpendicular to line $O'X'$ and QT perpendicular to OM. Thus, one has

$$O'N = O'M + MN = O'M + TQ = H\cos\alpha + x_P\sin\alpha \tag{11}$$

where $\alpha = \begin{cases} \pi - \tan^{-1}(v_x/v_z), & v_z > 0 \\ -\tan^{-1}(v_x/v_z), & v_z \le 0. \end{cases}$ Substituting (11) into (10) and after algebraic manipulation, one obtains

$$x_P = \frac{\lambda f_{\mathrm{id}} R_0}{2|\vec{v}|\sin\alpha} - H\cot\alpha. \tag{12}$$

Thus, x_P is a function of f_{id} and R_0. If f_{id} is known, x_P becomes a function of R_0 only. x_P is no longer an independent variable. Since P and P_{cen} are within the same instantaneous beam, then intuitively, we can set f_{id} of P being equal to the IDF of P_{cen} or the Doppler centroid (f_{dc}) of the return signal. Substituting f_{id} with f_{dc} in (12), one approximates

$$x_P = \frac{\lambda f_{\mathrm{dc}} R_0}{2|\vec{v}|\sin\alpha} - H\cot\alpha. \tag{13}$$

Thus, x_P is approximately one-to-one related to R_0. This approximation is feasible if the beamwidth is not very wide in the azimuth direction. In such case, the difference of f_{id} and f_{dc} is small. Therefore, with (13) and the first equation in (4), we have decoupled x_P and y_P from the phase term in (9). Thus, Φ can be re-expressed as $\Phi_{\mathrm{new}}(f_r, f_a, R_0)$, and the 2-D spectrum (9) can be re-expressed with only three variables as

$$S_{\mathrm{MSR\_new}}(f_r, f_a, R_0) = w_r(f_r)w_a(f_a)\exp\left[-j\pi\frac{f_r^2}{\gamma}\right] \times \exp\left[j\Phi_{\mathrm{new}}(f_r, f_a, R_0)\right]. \tag{14}$$

The spectrum for a SAR onboard a maneuverable platform with a curvilinear orbit is now similar in form to the spectrum for a SAR with a rectilinear orbit but with different content. An imaging algorithm that processes the spectrum with three variables can be used to focus the radar return. Before the implementation of the re-expressed spectrum into the imaging algorithm, one needs to understand the re-expressed spectrum further.

IV. Re-Expressed Spectrum

Φ_{new} in (14) can be expanded into a polynomial with respect to f_r. Since $S_{\mathrm{MSR\_new}}$ and S_{MSR} are of similar form, we directly use the expansion of S_{MSR} in [4] to expand Φ_{new} as

$$\Phi_{\mathrm{new}} = \phi_0(f_a; R_0) + \phi_1(f_a; R_0)f_r + \phi_2(f_a; R_0)f_r^2 + \cdots. \tag{15}$$

where ϕ_1 contains the range cell migration (RCM) and is

$$\begin{aligned}\phi_1(f_a; R_0) &= -4\pi\frac{R_0}{c} + \pi\frac{c}{4b_2}\left(4\left(\frac{b_1}{c}\right)^2 - \frac{f_a^2}{f_c^2}\right) \\ &\quad + \pi\frac{c^2 b_3}{16 b_2^3}\left[8\left(\frac{b_1}{c}\right)^3 - 2\frac{f_a^3}{f_c^3} - 6\frac{b_1}{c}\frac{f_a^2}{f_c^2}\right] + \pi\frac{c^3\left(9b_3^2 - 4b_2 b_4\right)}{256 b_2^5} \\ &\quad \times \left[-3\frac{f_a^4}{f_c^4} - 16\frac{1}{f_c^3}\frac{b_1}{c}f_a^3 - 24\frac{1}{f_c^2}\left(\frac{b_1}{c}\right)^2 f_a^2 + 16\left(\frac{b_1}{c}\right)^4\right].\end{aligned} \tag{16}$$

Equation (16) is generally complex but can be regrouped and expanded into another Taylor series at a reference range R_{ref}

$$\phi_1(f_a; R_0) = -4\pi\frac{R_0}{c} + \phi_\triangle(f_a; R_0) \approx -4\pi\frac{R_0}{c} + A(f_a; R_{\mathrm{ref}}) + B(f_a; R_{\mathrm{ref}})(R_0 - R_{\mathrm{ref}}) \tag{17}$$

where $A(f_a; R_{\mathrm{ref}})$ and $B(f_a; R_{\mathrm{ref}})$ are Taylor coefficients

$$\left.\begin{aligned} A(f_a; R_{\mathrm{ref}}) &= \phi_\Delta(f_a; R_0)\big|_{R_0 = R_{\mathrm{ref}}} \\ B(f_a; R_{\mathrm{ref}}) &= \left.\frac{\partial\phi_\Delta(f_a; R_0)}{\partial R_0}\right|_{R_0 = R_{\mathrm{ref}}} \end{aligned}\right\}. \tag{18}$$

The instantaneous range of P_{cen} at $t_m = 0$ is usually chosen as R_{ref}. With (17) the RCM can be written as

$$\begin{aligned} R(f_a, R_0) &= -\frac{c}{4\pi}\phi_1(f_a; R_0) = R_0 - \frac{c}{4\pi}A(f_a; R_{\mathrm{ref}}) \\ &\quad - \frac{c}{4\pi}B(f_a; R_{\mathrm{ref}})(R_0 - R_{\mathrm{ref}}) = R_0 + R_{\mathrm{res}} + a(f_a)R_0 \end{aligned} \tag{19}$$

with $R_{\mathrm{res}} = -(c/4\pi)[A(f_a; R_{\mathrm{ref}}) - B(f_a; R_{\mathrm{ref}})R_{\mathrm{ref}}]$ and $a(f_a) = -(c/4\pi)B(f_a; R_{\mathrm{ref}})$. In (19), the RCM is linearly related to R_0 so that the CS algorithm [7] can be applied to it. Then, the scaled RCM is

$$R_{\mathrm{CS}}(f_a; R_0) = R_0 + R_{\mathrm{res}} + a(f_a)R_{\mathrm{ref}}. \tag{20}$$

This equation indicates that, after the CS operation, targets of different R_0's have the same RCM curve as that of the reference target with R_{ref}. Thus, a bulk RCM correction could be carried out in the 2-D frequency domain to eliminate $R_{\mathrm{res}} + a(f_a)R_{\mathrm{ref}}$. Next, we implement and validate the decoupling method.

V. Implementation Into the CS Algorithm

In a typical CS algorithm, one starts with the transform of raw data in the time domain into the range–Doppler domain

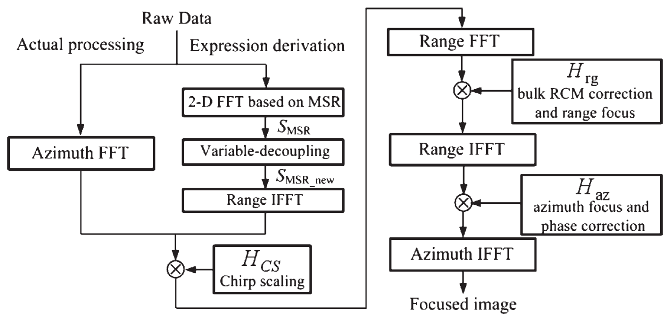

Fig. 3. Flow diagram of the variable-decoupling- and MSR-based CS algorithm.

TABLE I
SIMULATION PARAMETERS

Wavelength	0.02 m
Bandwidth	100 MHz
Oversampling ratio	1.5
Pulse duration	2 μs
Antenna size	1 m
PRF	8 kHz
H	9 km
$\vec{v}$	(1200, 0, –170) m/s
$\vec{a}$	(–10, 0, 5) m/s^2

(Fig. 3). However, with required decoupling, we need to apply an inverse Fourier transform in range to (14) to derive the expression in the range–Doppler domain

$$S(\hat{t}, f_a) = \exp\left[j\phi_0(f_a; R_0)\right] \times \exp\left[j\pi\gamma_e(f_a; R_0)\left(\hat{t} - \frac{2}{c}R(f_a; R_0)\right)^2\right] \quad (21)$$

with $(1/\gamma_e(f_a; R_0)) = (1/\gamma) - (\phi_2(f_a; R_0)/\pi)$ and amplitude ignored. Then, similar to the derivations in the CS algorithm [7], we obtain H_{CS}, H_{rg}, and H_{az} (Fig. 3) as

$$H_{\text{CS}} = \exp\left[j\pi\gamma_e(f_a; R_{\text{ref}})a(f_a) \times \left(\hat{t} - \frac{2}{c}\left(R_{\text{ref}} + a(f_a)R_{\text{ref}} + R_{\text{res}}\right)\right)^2\right] \quad (22)$$

$$H_{\text{rg}}(R_0, f_a) = \exp\left[j\frac{\pi}{\gamma_e(f_a; R_{\text{ref}})\left(a(f_a)+1\right)}f_r^2\right] \bullet \exp\left[j\frac{4\pi}{c}\left(a(f_a)R_{\text{ref}} + R_{\text{res}}\right)f_r\right] \quad (23)$$

$$H_{\text{az}}(R_0, f_a) = \exp\left[-j\phi_0(f_a; R_0)\right]\exp\left[-j\Theta_\Delta(f_a, R_0)\right] \quad (24)$$

with

$$\Theta_\Delta(f_a, R_0) = \pi\frac{4}{c^2}\gamma_e(f_a; R_{\text{ref}})\left(1 + a(f_a)\right)a(f_a) \times \left[(R_0 - R_{\text{ref}})^2 - 4R_{\text{ref}}R_{\text{res}}\right].$$

Next, simulations are carried out, and the results are discussed.

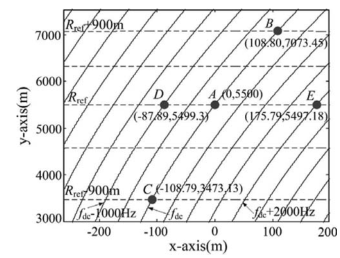

Fig. 4. Five ground targets A–E and their coordinates. Range contours are shown as dashed lines, and Doppler frequency contours are shown as curves at $t_m = 0$.

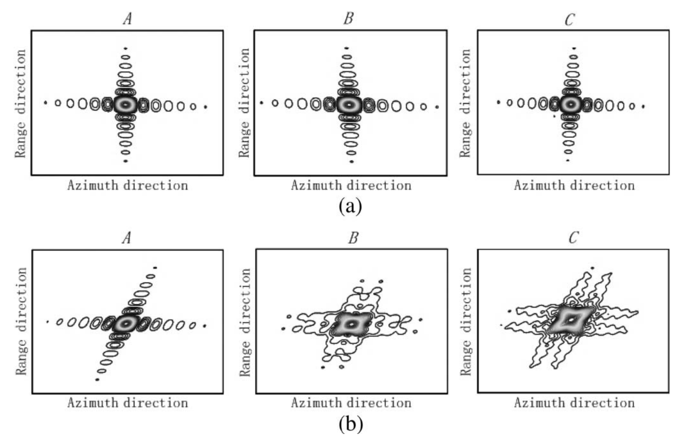

Fig. 5. Contours of the impulse responses from targets A–C using (a) this method and (b) the method in [4].

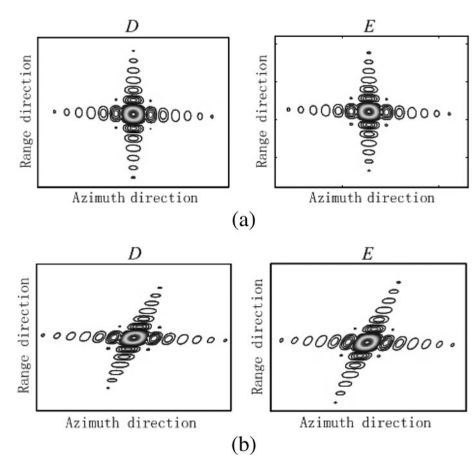

Fig. 6. Contours of the impulse responses from targets D and E using (a) this method and (b) the method in [4].

VI. SIMULATIONS AND RESULTS

The simulation parameters are given in Table I. The range resolution is 1.33 m, and the azimuth resolution is 0.44 m after the rectangular weighting with a factor of 0.886. Five ground targets A–E with their x and y coordinates are shown in Fig. 4. The footprint center of A is selected as the reference point P_{cen} with R_{ref} of 10 548 m. Fig. 4 shows the range contours (dashed lines) and IDF contours (curves) at $t_m = 0$. Targets B

TABLE II
IRW, PSLR, AND ISLR DATA FOR THE FIVE TARGETS USING THE DECOUPLING METHOD AND THE METHOD IN [4]. THE VALUES FROM THE METHOD IN [4] ARE IN PARENTHESES

Targets		*A*	*B*	*C*	*D*	*E*
Azimuth	IRW (m)	0.44 (0.45)	0.46 (0.57)	0.45 (0.64)	0.45 (0.45)	0.61 (0.61)
	PSLR (dB)	–13.35 (–13.35)	–13.35 (–18.61)	–13.35 (–23.39)	–13.25 (–13.07)	–12.72 (–12.80)
	ISLR (dB)	–10.36 (–10.37)	–10.82 (–15.67)	–10.28 (–18.46)	–10.12 (–10.00)	–10.01 (–10.10)
Range	IRW (m)	1.34 (1.5)	1.34 (1.56)	1.34 (2.13)	1.34 (1.34)	1.34 (1.34)
	PSLR (dB)	–13.28 (–17.53)	–13.26 (–18.39)	–13.23 (–31.8)	–13.28 (–13.29)	–13.25 (–13.26)
	ISLR (dB)	–9.92 (–16.91)	–9.85 (–13.82)	–10.01 (–25.62)	–9.92 (–9.92)	–9.90 (–9.90)

and C, as well as A, of the same IDF but at different ranges are chosen to test if the decoupling algorithm can handle a large imaging extent in the range direction. Targets D and E, and A, that have the same range but differ in IDFs are selected to see whether the algorithm can process a large azimuth extent.

The impulse responses of targets A, B, and C are shown as contours in the range and azimuth plane [Fig. 5(a)]. The responses are well focused with clear separations of the main lobes and first and subsequential sidelobes. For comparison, we also show the simulated outputs using the method in [4] in Fig. 5(b). The degree of the focusing of targets A–C indicates some deterioration. There are no clear delineations between the main lobes and sidelobes for B and C, although the delineation is clear for A.

The impulse responses of target D [Fig. 6(a)] are well focused in the range direction. However, defocusing occurs in the azimuth direction, which is caused by the difference in IDFs of D and A. The azimuth broadening is $\sim$4%, which is acceptable in SAR data processing. The impulse responses of target E might be similar to those of target D, but the azimuth defocusing worsens. The broadening is around 39% or unacceptable. The cause is directly related to the large distance between E and A as compared to the small distance of D and A. In contrast, the impulse responses of targets D and E [Fig. 6(b)] using the method by Yi *et al.* could be similar in focusing. Finally, the values of impulse response width (IRW), peak sidelobe ratio (PSLR), and integral sidelobe ratio (ISLR) in the range and azimuth directions are further used to assess both methods. Quantitatively, our method is generally superior to the method by Yi *et al.* (Table II). Consequently, with the incorporation of the decoupling method into the CS algorithm, promising results are obtained for a SAR onboard a maneuverable platform.

VII. CONCLUSION

For an echo acquired by a SAR with a curvilinear track, we have developed a variable-decoupling method to decouple the x and y coordinates in the 2-D spectrum of the echo on the basis of an imaging geometry of the curvilinear track and using the concept of IDF. The decoupling was done through the reparameterization of x or y solely as a function of the instantaneous distance between the sensor and the target at zero azimuth time (R_0), as well as the position, attitude, and system parameters of the SAR. Equivalently, only the range frequency, azimuth frequency, and R_0 remained in the 2-D spectrum after decoupling. Then, we implemented the decoupling method into a widely used CS imaging algorithm. Promising results from targets spread widely in the range and azimuth dimensions were obtained in the simulations.

REFERENCES

[1] M. Xing, X. Jiang, R. Wu, F. Zhou, and Z. Bao, “Motion compensation for UAV SAR based on raw radar data,” *IEEE Trans. Geosci. Remote Sens.*, vol. 47, no. 8, pp. 2870–2883, Aug. 2009.

[2] T. Michel and S. Hensley, “Wavenumber domain focusing of squinted SAR data with a curved orbit geometry,” in *Proc. 42nd Asilomar Conf. Signals, Syst. Comput.*, Pacific Grove, CA, Oct. 2008, pp. 26–29.

[3] Y. L. Neo, F. H. Wong, and I. G. Cumming, “A two-dimensional spectrum for bistatic SAR processing using series reversion,” *IEEE Geosci. Remote Sens. Lett.*, vol. 4, no. 1, pp. 93–96, Jan. 2007.

[4] Y. Yi, L. Zhang, X. Liu, N. Liu, and S. Dong, “An efficient imaging algorithm for missile-borne side-looking SAR,” in *Proc. IET Int. Radar Conf.*, Guilin, China, Apr. 2009, pp. 20–22.

[5] I. G. Cumming and F. H. Wong, *Digital Processing of Synthetic Aperture Radar: Algorithms and Implementation*. Norwood, MA: Artech House, 2004.

[6] P. Zhou, S. Zhou, T. Xiong, Y. Li, and M. Xing, “A novel high resolution imaging method for the missile-borne SAR,” (in Chinese), *J. Electron. Inf. Technol.*, vol. 33, no. 3, pp. 622–627, Mar. 2011.

[7] R. K. Raney, H. Runge, R. Bamler, I. G. Cumming, and F. H. Wong, “Precision SAR processing using chirp scaling,” *IEEE Trans. Geosci. Remote Sens.*, vol. 32, no. 4, pp. 786–799, Jul. 1994.